

# Operando Evolution of the Structure and Oxidation State of Size-Controlled Zn Nanoparticles during CO<sub>2</sub> Electroreduction

Hyo Sang Jeon,<sup>†</sup> Ilya Sinev,<sup>†</sup> Fabian Scholten,<sup>†</sup> Nuria J. Divins,<sup>†</sup> Ioannis Zegkinoglou,<sup>†,‡</sup> Lukas Pielsticker,<sup>†</sup> and Beatriz Roldan Cuenya<sup>\*,†,§,ⓑ</sup>

<sup>†</sup>Department of Physics, Ruhr-University Bochum, 44780 Bochum, Germany

<sup>§</sup>Department of Interface Science, Fritz-Haber-Institute of the Max-Planck Society, 14195 Berlin, Germany

## Supporting Information

**ABSTRACT:** We explored the size-dependent activity and selectivity of Zn nanoparticles (NPs) for the electrochemical CO<sub>2</sub> reduction reaction (CO<sub>2</sub>RR). Zn NPs ranging from 3 to 5 nm showed high activity and selectivity (~70%) for CO production, whereas those above 5 nm exhibited bulk-like catalytic properties. In addition, a drastic increase in hydrogen production was observed for the Zn NPs below 3 nm, which is associated with the enhanced content of low-coordinated sites on small NPs. The presence of residual cationic Zn species in the catalysts was also revealed during CO<sub>2</sub>RR via *operando* X-ray absorption fine-structure spectroscopy measurements. Such species are expected to play a role in the selectivity trends obtained. Our findings can serve as guidance for the development of highly active and CO-selective Zn-based catalysts for CO<sub>2</sub>RR.

Developing electrocatalysts for the CO<sub>2</sub> electrochemical reduction reaction (CO<sub>2</sub>RR) has attracted much attention as promising means to produce useful chemicals and fuels.<sup>1</sup> Several metal electrodes such as Au,<sup>2,3</sup> Ag,<sup>4</sup> Pd,<sup>5</sup> and Zn<sup>6</sup> have been identified to electrochemically reduce CO<sub>2</sub> into CO. Carbon monoxide is an important raw chemical in a number of industrial processes such as Fischer–Tropsch reactions.<sup>1,6</sup> Zn is a promising material for CO<sub>2</sub>RR due to its low price and earth abundance. Unfortunately, it is considerably less reactive than Au and Ag.

One way to improve catalytic activity is to synthesize catalysts in the form of nanoparticles (NPs) in order to increase the surface-to-volume ratio.<sup>7</sup> Moreover, recent studies on size-controlled metal NPs have revealed the strong structure-sensitivity of CO<sub>2</sub>RR.<sup>8–10</sup> For example, the activity and selectivity of Cu and Au NPs for H<sub>2</sub> and CO was found to increase drastically with decreasing NP size, whereas for Cu NPs hydrocarbon selectivity was suppressed. This trend was assigned to an increase in the population of low-coordinated surface sites.<sup>9,10</sup>

Several experimental and computational studies have indicated that modifications in the structure and morphology of Zn surfaces can lead to an improved CO<sub>2</sub>RR activity and CO selectivity.<sup>11–14</sup> For example, Zn catalysts with hexagonal shapes from Won et al. showed 60 times higher CO partial current densities than those of the Zn foil.<sup>14</sup> According to their DFT calculations, rough Zn(101) facets favor CO production

from CO<sub>2</sub> at lower potentials and display a higher energy barrier for HER than smooth Zn(002) facets.<sup>14</sup> Although these results indicate that the reactivity of Zn catalysts for CO<sub>2</sub>RR strongly correlates with their structure, in depth understanding of the origin of such correlation is still missing. Work on structurally and chemically well-defined nanostructures is still needed to clarify the specific role of low-coordinated sites at the surface,<sup>15,16</sup> grain boundaries,<sup>17,18</sup> or the oxidation state of the catalysts under reaction conditions,<sup>19–23</sup> and how they contribute to the final activity and selectivity trends observed.

In this study, size-controlled Zn NPs were synthesized via inverse micelle encapsulation in PS-P2VP diblock copolymers. Their morphology was investigated via atomic force microscopy (AFM), Figure 1. The Zn NPs were dip-coated on smooth silicon wafers for a more accurate NP height determination. The average Zn NP sizes ranged from 1.7 to 6.8 nm and a uniform arrangement on the substrate was observed. The corresponding histograms are shown in Figure

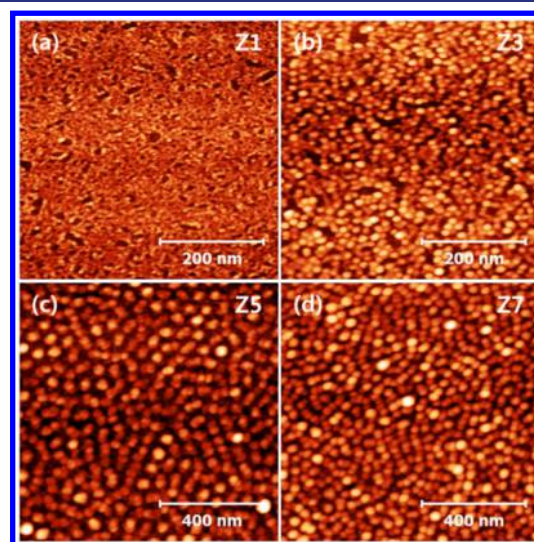


**Figure 1.** AFM images of Zn NP samples prepared via inverse micelle encapsulation and supported on SiO<sub>2</sub>/Si(111). (a) Zn1 (1.7 ± 0.4 nm), (b) Zn3 (2.9 ± 0.7 nm), (c) Zn5 (4.5 ± 1.2 nm), and (d) Zn7 (6.8 ± 1.6 nm).

Received: May 19, 2018

Published: July 15, 2018

S1, and a summary of the synthesis parameters and AFM analysis results in Table S1.

In order to gain insight into the structure and chemical state of the Zn NPs during CO<sub>2</sub>RR, X-ray absorption fine-structure spectroscopy (XAFS) measurements were carried out under *operando* conditions at  $-1.1$  V vs RHE in aqueous CO<sub>2</sub>-saturated 0.1 M KHCO<sub>3</sub>. Figure 2 shows X-ray absorption

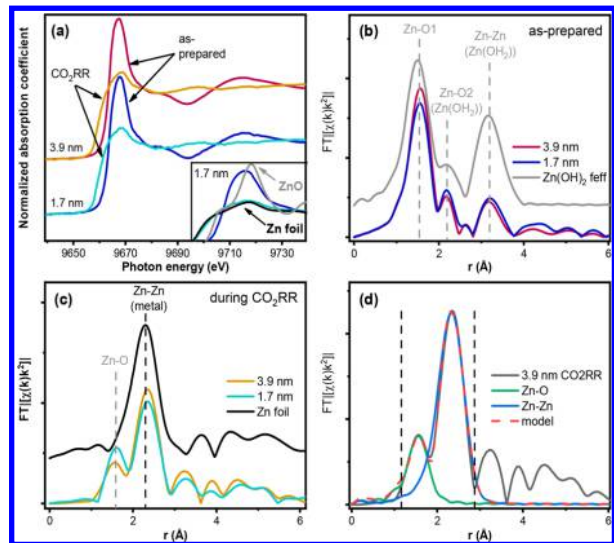


**Figure 2.** (a) Zn K-edge XANES data from 1.7 and 3.9 nm Zn NPs acquired in air and under *operando* CO<sub>2</sub>RR conditions at  $-1.1$  V vs RHE in 0.1 M KHCO<sub>3</sub>. The inset shows the white line region of the 1.7 nm NPs together with bulk Zn and ZnO references. (b and c) Fourier-transformed  $k^2$ -weighted EXAFS spectra of the same samples. Bulk Zn and an orthorhombic Zn(OH)<sub>2</sub> structure modeled by FEFF are plotted as reference.<sup>30</sup> (d) 1st shell analysis of the EXAFS spectrum of 3.9 nm NPs during CO<sub>2</sub>RR. Dashed vertical lines show the limits of the fit.

near-edge (XANES) and extended X-ray absorption fine-structure spectra (EXAFS) of Zn NP samples with average sizes of 1.7 (Zn1) and 3.9 nm (Zn4), measured at the Zn K-edge.

Notably, the XANES spectra of the as-prepared Zn NPs (Figure 2a) show distinct differences with respect to bulk ZnO with wurtzite structure as well as Zn acetate used as precursor in the NPs synthesis.<sup>24,25</sup> The absorption edge position is shifted by ca. 3.5 eV to higher energy, whereas the first absorption feature above the edge, so-called “white line”, is considerably broader than the one of the ZnO reference and does not have a characteristic shoulder at ca. 9663 eV. These observations allow us to conclude that Zn atoms in the as-prepared NPs likely have octahedral coordination, rather than tetrahedral typical for ZnO and Zn(Ac)<sub>2</sub>.<sup>26,27</sup> Moreover, a similar spectral shape was reported for small ZnO clusters of octahedral structure with size below 3 nm and solvated Zn ions.<sup>27,28</sup> Zn undergoes significant reduction during CO<sub>2</sub>RR as indicated by the lower white line intensity in the XANES spectra (Figure 2a). However, those zinc oxide species do not become completely reduced under CO<sub>2</sub>RR, as evidenced by a slightly higher white line in XANES spectra compared to the Zn foil.

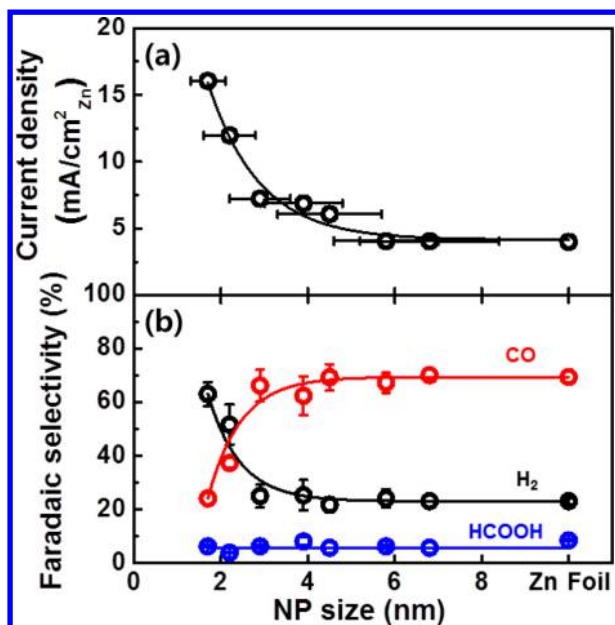
The EXAFS spectra of the as-prepared NPs (Figure 2b) show the presence of Zn–O bonds at  $\sim 1.55$  Å (uncorrected for phase shift), with coordination numbers (CN) ranging from  $1.7 \pm 0.4$  to  $1.9 \pm 0.3$ , depending on the particle size (see

Table S2). In addition, there is a shoulder at 2.17 Å (uncorrected), which cannot be assigned either to Zn–Zn in metallic Zn, or to Zn–C in a Zn(Ac)<sub>2</sub> structure due to a significant shift. An orthorhombic Zn(OH)<sub>2</sub> structure<sup>29</sup> was found to fit best such feature, with a second Zn–O backscattering appearing at 2.65 Å and coordination numbers of  $1.9 \pm 0.6$  and  $2.1 \pm 0.7$  for Zn1 (1.7 nm) and Zn4 (3.9 nm), correspondingly (Table S2). The fitted coordination numbers of the as-prepared NPs were very similar for all samples of different initial AFM size. These results indicate the presence of Zn(OH)<sub>2</sub> clusters of well-defined crystalline structure in all samples before reduction.

During CO<sub>2</sub>RR, a metallic Zn–Zn backscattering feature emerges at 2.35 Å (uncorrected) in the EXAFS spectra (Figure 2c). Furthermore, the intensity of the former feature changes according to the NP size, with coordination numbers of  $4.8 \pm 0.9$  and  $4.1 \pm 0.8$  obtained for the NPs with sizes of 3.9 and 1.7 nm, correspondingly. This is in agreement with the larger disorder expected for the smallest NPs as compared to bulk Zn (CN=6). However, complete NP reduction was not observed, as corroborated by the presence of oxygen in the Zn local environment (feature at 1.53 Å, uncorrected). A Zn–O fraction with CN  $0.5 \pm 0.2$  was obtained for the 3.9 nm NPs and  $0.6 \pm 0.2$  for the 1.7 nm NPs. Increasing Zn–O CN with decreasing NP size indicates that the larger amount of the undercoordinated sites available in small NPs is able to better stabilize the oxidic Zn species. Moreover, a peak at 3.2 Å (uncorrected), corresponding to the first Zn–Zn scattering in Zn(OH)<sub>2</sub> persists under reaction conditions, thus indicating that zinc hydroxide species remain stable under CO<sub>2</sub>RR.

To complement the XAFS characterization, surface-sensitive quasi *in situ* XPS measurements were carried out, Figure S4. The electrochemical cell used is directly attached to a UHV system equipped with XPS for sample transfer without air exposure. The XPS results confirm the presence of Zn(OH)<sub>2</sub> species on the surface of the as-prepared samples. They also demonstrate that such species are still present on the samples after CO<sub>2</sub>RR. Since the latter could be partially a result of post-reaction rehydroxylation of the sample surface due to contact with leftover aqueous electrolyte, we consider the *operando* XAFS measurements as the most reliable source of information about the structure and composition of the catalysts under reaction conditions. The latter clearly show the coexistence of cationic species (with a structure resembling that of Zn hydroxides) and metallic Zn during CO<sub>2</sub>RR.

Activity and selectivity CO<sub>2</sub>RR measurements were performed on Zn NPs supported on glassy carbon at a constant potential of  $-1.1$  V vs RHE in a CO<sub>2</sub>-saturated 0.1 M KHCO<sub>3</sub> aqueous electrolyte. The data were normalized by the geometric Zn surface area estimated for spherical NPs using the AFM NP height as characteristic size parameter. This was done after subtraction of the glassy carbon background. As shown in Figure 3a, we could confirm an increase in the total catalytic activity with decreasing Zn NP size. To be more specific, all samples with size below 5 nm exhibited higher activity than the Zn foil, whereas large NPs (Zn6 and Zn7) showed comparable activity to bulk Zn. A factor-of-four improvement in the catalytic activity of our smallest NPs (1.7 nm, Zn1) was obtained as compared to Zn7 (6.8 nm). In addition, H<sub>2</sub> and CO were detected as major products in all samples, with about 5% of formic acid as minor product (Figure 3b). Similar selectivity toward CO of  $\sim 70\%$  was observed for all NPs larger than 3 nm, which is comparable to



**Figure 3.** Activity and selectivity measurements of CO<sub>2</sub>RR over Zn NPs. (a) Current densities and (b) Faradaic selectivity toward H<sub>2</sub>, CO and HCOOH measured at  $-1.1$  V vs RHE in  $0.1$  M KHCO<sub>3</sub> as a function of the Zn NP size.

the selectivity of Zn foils. Interestingly, the H<sub>2</sub> selectivity from the parasitic hydrogen evolution reaction (HER) was significantly increased for NP sizes below 3 nm, whereas CO production was abruptly suppressed. These results indicate that activity and selectivity for CO<sub>2</sub> reduction exhibit a clear size effect on Zn NPs.

On the basis of these results, we could separate the activity and selectivity trends during CO<sub>2</sub>RR in three different NP size regimes: (i) below 3 nm, high activity and low CO selectivity was observed; (ii) between 3 and 5 nm, the NPs are more active than bulk Zn while preserving a similar selectivity; (iii) over 5 nm, a decrease in the activity is seen while the CO selectivity remains high and nearly constant. This is in agreement with previous DFT work on Au NPs<sup>10</sup> reporting that high H coverages are expected on small NPs due to the enhanced fraction of low-coordinated sites, and that under such conditions the binding of reaction intermediates such as COOH\* is weakened, leading to a lower CO production versus H<sub>2</sub>.<sup>10</sup>

Our discovery of cationic Zn species under CO<sub>2</sub>RR conditions suggests that such species may be directly involved in the CO<sub>2</sub>RR pathway. Recently, Nguyen et al. suggested that the high performance of their Zn nanocatalysts with porous structure could be related to the presence of oxidized Zn species.<sup>31</sup> Nevertheless, no *operando* or *in situ* data were available to substantiate their claim. Other researches have also reported that metal catalysts such as In and Sn are not fully reduced under CO<sub>2</sub>RR, and that the remaining metal oxides directly affect the activity and selectivity.<sup>32–35</sup> This work reveals that our Zn-based catalysts are not completely reduced to metallic Zn even under strongly negative potentials during CO<sub>2</sub>RR. However, further investigation is still needed to elucidate the specific role of the cationic Zn species in the reaction mechanism.

Lastly, it should be noted that the size effect on the selectivity of CO<sub>2</sub>RR was negligible for NPs larger than 3 nm,

which suggests that changes in the structure of large NPs or nanostructured surfaces<sup>11–14</sup> cannot be solely responsible for the distinct selectivity trends observed. Instead, one should consider additional factors such as the local pH, which indirectly also depends on the local morphology of the active sites. For instance, the rate of H<sub>2</sub> production is highly sensitive to the local pH and buffer composition of the electrolyte.<sup>36</sup> In addition, we have confirmed the presence of cationic Zn species, with a structure resembling that of Zn(OH)<sub>2</sub>, in the catalysts during the reaction, which is also expected to play a role in the enhanced performance of the modified Zn catalysts. Interestingly, adsorbed chlorine ions on the catalysts were also discussed to affect the CO<sub>2</sub>RR selectivity.<sup>12,14,31</sup> As a result, it appears that Zn catalysts seem to display a better performance when their chemical state/electronic properties are modified, rather than by exclusively changing their morphology.

In summary, a clear size-dependent trend in CO<sub>2</sub>RR over Zn NPs was observed, with NPs smaller than 3 nm being more active but less selective for CO in favor of H<sub>2</sub>. Moreover, CO selectivity of Zn NPs with sizes above 3 nm was similar to that of bulk Zn. Thus, a clear correlation between the coordination number of surface atoms and the catalytic performance could be inferred. Furthermore, our work reveals that CO<sub>2</sub>RR selectivity can be tuned not only by altering the structure or morphology of the Zn catalyst but also by the stabilization of cationic Zn species under reaction conditions. Our findings are relevant for the rational design of more efficient and cost-effective CO<sub>2</sub> reduction catalysts.

## ■ ASSOCIATED CONTENT

### 📄 Supporting Information

The Supporting Information is available free of charge on the ACS Publications website at DOI: 10.1021/jacs.8b05258.

Experimental details, synthesis parameters and AFM characterization of the Zn NPs, additional analysis of the *operando* XAFS data and quasi *in situ* XPS data (PDF)

## ■ AUTHOR INFORMATION

### Corresponding Author

\*Roldan@fhi-berlin.mpg.de

### ORCID

Ioannis Zegkinoglou: 0000-0002-1101-6935

Beatriz Roldan Cuenya: 0000-0002-8025-307X

### Notes

The authors declare no competing financial interest.

## ■ ACKNOWLEDGMENTS

This work was funded by the German Federal Ministry of Education and Research (BMBF) under grant #03SF0523C (CO2EKAT) and the ERC OPERANDOCAT (ERC-725915). The authors gratefully acknowledge the CLAES beamline staff for their support and ALBA synchrotron light source for the XAFS beamtime.

## ■ REFERENCES

- (1) Whipple, D. T.; Kenis, P. J. A. *J. Phys. Chem. Lett.* **2010**, *1*, 3451.
- (2) Liu, M.; Pang, Y.; Zhang, B.; De Luna, P.; Voznyy, O.; Xu, J.; Zheng, X.; Dinh, C. T.; Fan, F.; Cao, C.; de Arquer, F. P. G.; Safaei, T. S.; Mepham, A.; Klinkova, A.; Kumacheva, E.; Filleter, T.; Sinton, D.; Kelley, S. O.; Sargent, E. H. *Nature* **2016**, *537*, 382.
- (3) Chen, Y.; Li, C. W.; Kanan, M. W. *J. Am. Chem. Soc.* **2012**, *134*, 19969.

- (4) Kim, C.; Jeon, H. S.; Eom, T.; Jee, M. S.; Kim, H.; Friend, C. M.; Min, B. K.; Hwang, Y. J. *J. Am. Chem. Soc.* **2015**, *137*, 13844.
- (5) Gao, D.; Zhou, H.; Wang, J.; Miao, S.; Yang, F.; Wang, G.; Wang, J.; Bao, X. *J. Am. Chem. Soc.* **2015**, *137*, 4288.
- (6) Hori, Y. In *Modern Aspects of Electrochemistry*; Vayenas, C. G., White, R. E., Gamboa-Aldeco, M. E., Eds.; Springer: New York, 2008; Vol. 42.
- (7) Moshfegh, A. Z. *J. Phys. D: Appl. Phys.* **2009**, *42*, 233001.
- (8) Mistry, H.; Reske, R.; Strasser, P.; Roldan Cuenya, B. *Catal. Today* **2017**, *288*, 30.
- (9) Reske, R.; Mistry, H.; Behafarid, F.; Roldan Cuenya, B.; Strasser, P. *J. Am. Chem. Soc.* **2014**, *136*, 6978.
- (10) Mistry, H.; Reske, R.; Zeng, Z.; Zhao, Z.-J.; Greeley, J.; Strasser, P.; Roldan Cuenya, B. *J. Am. Chem. Soc.* **2014**, *136*, 16473.
- (11) Jiang, X.; Cai, F.; Gao, D.; Dong, J.; Miao, S.; Wang, G.; Bao, X. *Electrochem. Commun.* **2016**, *68*, 67.
- (12) Quan, F.; Zhong, D.; Song, H.; Jia, F.; Zhang, L. *J. Mater. Chem. A* **2015**, *3*, 16409.
- (13) Rosen, J.; Hutchings, G. S.; Lu, Q.; Forest, R. V.; Moore, A.; Jiao, F. *ACS Catal.* **2015**, *5*, 4586.
- (14) Won, D. H.; Shin, H.; Koh, J.; Chung, J.; Lee, H. S.; Kim, H.; Woo, S. I. *Angew. Chem., Int. Ed.* **2016**, *55*, 9297.
- (15) Louidice, A.; Lobaccaro, P.; Kamali, E. A.; Thao, T.; Huang, B. H.; Ager, J. W.; Buonsanti, R. *Angew. Chem., Int. Ed.* **2016**, *55*, 5789.
- (16) Roberts, F. S.; Kuhl, K. P.; Nilsson, A. *Angew. Chem.* **2015**, *127*, 5268–5271.
- (17) Verdaguer-Casadevall, A.; Li, C. W.; Johansson, T. P.; Scott, S. B.; McKeown, J. T.; Kumar, M.; Stephens, I. E. L.; Kanan, M. W.; Chorkendorff, I. *J. Am. Chem. Soc.* **2015**, *137*, 9808–9811.
- (18) Feng, X.; Jiang, K.; Fan, S.; Kanan, M. W. *J. Am. Chem. Soc.* **2015**, *137*, 4606.
- (19) Mistry, H.; Varela, A. S.; Kühl, S.; Strasser, P.; Roldan Cuenya, B. *Nat. Rev. Mater.* **2016**, *1*, 16009.
- (20) Mistry, H.; Varela, A. S.; Bonifacio, C. S.; Zegkinoglou, I.; Sinev, I.; Choi, Y.-W.; Kisslinger, K.; Stach, E. A.; Yang, J. C.; Strasser, P.; Roldan Cuenya, B. *Nat. Commun.* **2016**, *7*, 12123.
- (21) Mistry, H.; Choi, Y.-W.; Bagger, A.; Scholten, F.; Bonifacio, C. S.; Sinev, I.; Divins, N. J.; Zegkinoglou, I.; Jeon, H. S.; Kisslinger, K.; Stach, E. A.; Yang, J. C.; Rossmeisl, J.; Roldan Cuenya, B. *Angew. Chem., Int. Ed.* **2017**, *56*, 11394.
- (22) Favaro, M.; Xiao, H.; Cheng, T.; Goddard, W. A.; Yano, J.; Crumlin, E. J. *Proc. Natl. Acad. Sci. U. S. A.* **2017**, *114*, 6706.
- (23) Cheng, T.; Xiao, H.; Goddard, W. A. *Proc. Natl. Acad. Sci. U. S. A.* **2017**, *114*, 1795.
- (24) Grady, B. P.; Floyd, J. A.; Genetti, W. B.; Vanhoorne, P.; Register, R. A. *Polymer* **1999**, *40*, 283.
- (25) Ishioka, T.; Maeda, K.; Watanabe, I.; Kawauchi, S.; Harada, M. *Spectrochim. Acta, Part A* **2000**, *56*, 1731.
- (26) Pan, H. K.; Knapp, G. S.; Cooper, S. L. *Colloid Polym. Sci.* **1984**, *262*, 734.
- (27) Waychunas, G. A.; Fuller, C. C.; Davis, J. A.; Rehr, J. J. *Geochim. Cosmochim. Acta* **2003**, *67*, 1031.
- (28) Kuzmin, A.; Larcheri, S.; Rocca, F. *J. Phys.: Conf. Ser.* **2007**, *93*, 012045.
- (29) Corey, R.; Wyckoff, R. Z. *Kristallogr. - Cryst. Mater.* **1933**, *86*, 8.
- (30) Ankudinov, A. L.; Ravel, B.; Rehr, J. J.; Conradson, S. D. *Phys. Rev. B: Condens. Matter Mater. Phys.* **1998**, *58*, 7565.
- (31) Nguyen, D. L. T.; Jee, M. S.; Won, D. H.; Jung, H.; Oh, H.; Min, B. K.; Hwang, Y. J. *ACS Sustainable Chem. Eng.* **2017**, *5*, 11377.
- (32) Chen, Y.; Kanan, M. W. *J. Am. Chem. Soc.* **2012**, *134*, 1986.
- (33) Baruch, M. F.; Pander, J. E.; White, J. L.; Bocarsly, A. B. *ACS Catal.* **2015**, *5*, 3148.
- (34) Pander, J. E.; Baruch, M. F.; Bocarsly, A. B. *ACS Catal.* **2016**, *6*, 7824.
- (35) Dutta, A.; Kuzume, A.; Rahaman, M.; Vesztergom, S.; Broekmann, P. *ACS Catal.* **2015**, *5*, 7498.
- (36) Wuttig, A.; Yaguchi, M.; Motobayashi, K.; Osawa, M.; Surendranath, Y. *Proc. Natl. Acad. Sci. U. S. A.* **2016**, *113*, No. E4858.